Rapid Communications

Origin of the high Seebeck coefficient of the misfit $[Ca_2CoO_3]_{0.62}[CoO_2]$ cobaltate from site-specific valency and spin-state determinations

Abdul Ahad,[1] K. Gautam,[2] S. S. Majid,[1,*] S. Francoual,[3] F. Rahman,[1] Frank M. F. De Groot,[4] and D. K. Shukla[2,†]

[1]*Department of Physics, Aligarh Muslim University, Aligarh 202002, India*

[2]*UGC-DAE Consortium for Scientific Research, Indore 452001, India*

[3]*Deutsches Elektronen-Synchrotron, Notkestrasse 85, D-22607 Hamburg, Germany*

[4]*Debye Institute for Nanomaterials Science, Utrecht University-99, 3584 CG Utrecht, The Netherlands*

(Received 3 April 2020; revised manuscript received 1 June 2020; accepted 3 June 2020; published 16 June 2020)

Layered misfit cobaltate $[Ca_2CoO_3]_{0.62}[CoO_2]$, which emerged as an important thermoelectric material [A. C. Masset *et al.* Phys. Rev. B **62**, 166 (2000)], has been explored extensively in the last decade for the exact mechanism behind its high Seebeck coefficient. Its complex crystal and electronic structures have inhibited consensus among such investigations. This situation has arisen mainly due to difficulties in accurate identification of the chemical state, spin state, and site symmetries in its two subsystems (rocksalt $[Ca_2CoO_3]$ and triangular $[CoO_2]$). By employing resonant photoemission spectroscopy and x-ray absorption spectroscopy along with charge transfer multiplet simulations (at the Co ions), we have successfully identified the site symmetries, valencies, and spin states of the Co in both layers. Our site-symmetry observations explain the experimental value of the high Seebeck coefficient and also confirm that the carriers hop within the rocksalt layer, which is in contrast to earlier reports where hopping within triangular CoO_2 layer has been held responsible for the large Seebeck coefficient.

DOI: 10.1103/PhysRevB.101.220202

Materials that can convert heat into electricity are often called thermoelectric materials. A good thermoelectric material should possess low thermal conductivity (κ), high Seebeck coefficient (S), and high electrical conductivity (σ) to provide the maximum value of figure of merit ZT ($S^2\,\sigma/\kappa$). The cobalt-based layered-structure family (Na_xCoO_2, $Bi_2Sr_2Co_2O_9$, and $Ca_3Co_4O_9$) fulfilling the above-mentioned requirements has become popular. Especially the cobaltates, Na_xCoO_2 [1] and $Bi_2Sr_2Co_2O_9$ [2], with the triangular CoO_2 lattice, which is made up of edge-shared trigonal symmetric CoO_6 octahedra, have gathered much attraction. The former is very well studied because of its unique properties like superconductivity in the hydrated form [1,3] and high S value for $x = 0.5$ composition [4]. The later one also has a high S value and its properties were explored using several techniques such as photoemission and absorption spectroscopies [2]. The discovery of large S in Na_xCoO_2 opened a path for researchers to make efforts in these structures. The chemical stability of the thermoelectric materials at high temperatures is also a common issue from the application point of view and this restricts the use of Na.

Earlier, $Ca_3Co_4O_9$ (CCO) emerged as an important candidate for thermoelectricity from the misfit cobaltate family with stability up to high temperatures [5]. Its crystal structure comprises two incommensurately modulated subsystems sharing the same *a* and *c* but different *b* lattice parameters (for details, see the Supplemental Material [6] and references [7,8] therein). The chemical structure of CCO (precise chemical formula $[Ca_2CoO_3]_{0.62}[CoO_2]$) is similar to that of Na_xCoO_2 and can be compared with its $x = 2/3$ composition. In CCO, the layer CoO_2 is presumed to be conducting and the rocksalt layer Ca_2CoO_3 insulating, as is suggested from studies on other isostructural compounds [2,9]. Mixed valency of Co^{3+} and Co^{4+} is reported by x-ray photoemission and absorption spectroscopy [9,10] and the Heikes formula was employed to calculate S values which was first used by Koshibae *et al.* [4] for explaining the S value, in high temperature, for mixed valent cobaltates. However, the origin of large S in this compound is controversial and has been proposed in different ways. By electron-energy-loss spectroscopy measurements, it was shown that to maintain charge neutrality, holes from the rocksalt layers transfer into the CoO_2 layer and increase the concentration of mobile holes in it, which enables high S (Ref. [11]). Also, using $2p$-$3d$ resonant photoemission spectroscopy (RPES), it is reported [12] that the Co $3d$ and O $2p$ hybridized states are spread from E_F up to 8 eV and S has been calculated using Boltzmann metallic conduction with extended band, not by the Heikes formula. Moreover, theoretically, application of the Heikes formula is reported in rocksalt [13] as well as in the CoO_2 layer, [14,15] and these controversies continue because of the lack of experimental evidence.

Note that the Co valency estimation from an approximate chemical formula ($Ca_3Co_4O_9$) gives Co in +3 oxidation state, while in the misfit form the chemical formula contains CoO_2 and Ca_2CoO_3, which, individually, supposedly contain Co ions in +4 and +2 states, respectively. However, on comparing its actual chemical formula $[Ca_2CoO_3]_{0.62}[CoO_2]$ with

*Present address: Optical Physics Lab, Institute of Physics, Academia Sinica, Taipei, Taiwan.

†Corresponding author: dkshukla@csr.res.in

equivalent $Na_{2/3}CoO_2$, one gets a clue that the cobalt in CoO_2 layers has a +3.34 oxidation state and +3.05 in the rocksalt layer. This suggests that the holes should transfer from the CoO_2 to the rocksalt layer but the scenario reported [11] is contrary to this. Unfortunately, no direct tool exists that can estimate the correct valency in these two subsystems. The literature also contains controversies regarding the spin states of the Co^{3+} and the Co^{4+} ions and also which layer is the conducting layer-rocksalt or triangular.

In this Rapid Communication, we address the above issues and unravel the observation of different valency and spin states in rocksalt and the CoO_2 layers by utilizing the symmetry as a distinction tool for two subsystems. The results are unique and provide evidence of the presence of both D_{3d} and D_{4h} symmetries. Cobalt ions in mixed spin states [high-spin state (HSS) + low-spin state (LSS)] and +3/+4 valency are found to play an important role in the rocksalt layer for the high Seebeck coefficient. We also confirm that density of states (DOS) of the triangular layer is adjacent to E_F and contains Co in +3 only. Based on our results of chemical states and spins states in both these layers, we have employed the Heikes formula in rocksalt and calculated value of S is in excellent agreement with the experimental value.

Polycrystalline CCO has been synthesized using a solid-state route using the postcalcination method [16]. X-ray diffraction (XRD) has been performed at P09, DESY, Germany with 0.539 Å wavelength using an image plate detector (Perkin Elmer XRD1621 detector having 40 × 40 cm^2 active area with 2048 × 2048 pixels). Single-phase synthesis is confirmed by Rietveld refinement using monoclinic superspace group $C2/m(0b0)00$, where $b = 1.612$ is the structural modulation vector [17] (see Supplemental Material [6] Figs. S1 and S2). Magnetic susceptibility and resistivity has been measured as a function of temperature to confirm the quality of the sample [see Figs. S3(a) and S3(b) [6]]. X-ray photoemission spectroscopy (XPS) has been carried out using an Omicron energy analyzer (EA-125) with Al $K\alpha$ (1486.6 eV) x-ray source. Valence band spectra (VBS) with the incident photon energies in the range of 44-68 eV were recorded at BL-02 of Indus-1 synchrotron, RRCAT, India. The experimental resolution in this photon energy range was estimated to be ∼0.3 − 0.4 eV. The X-ray absorption spectroscopy (XAS) experiments were performed at BL-01 of Indus-2 synchrotron, RRCAT, India. In the XAS experiments, energy resolution at the Co $L_{3,2}$ edges was ∼0.3 eV.

Figure 1(a) shows the Rietveld refined XRD pattern of CCO. Inset shows the supercell (a, $13b$, c) comprising both subsystems (see Figs. S1 and S2 and related text [6]). It shows the cobalt environments in the triangular CoO_2 layer and rocksalt layer. Fitted Co $2p$ and O $1s$ core XPS are displayed in Figs. 1(b) and 1(c). XPS fitting reveals the +3 (∼68%) and +4 (∼32%) oxidation states of the cobalt ion in CCO. Therefore, average cobalt valency is found to be +3.32. The O $1s$ XPS shows lattice oxygen deficiency which may act as an electron doping at the cobalt sites in the rocksalt layer i.e., $[Ca_2CoO_{3-\delta}]_{0.62}[CoO_2]$. The mixed valency cannot tell which layer contains how much proportion of an oxidation state (+3 or +4) nor about the spin states.

In literature, previous reports have shown the Co^{3+} and Co^{4+} in LSSs [9,14]. Generalized gradient approximation

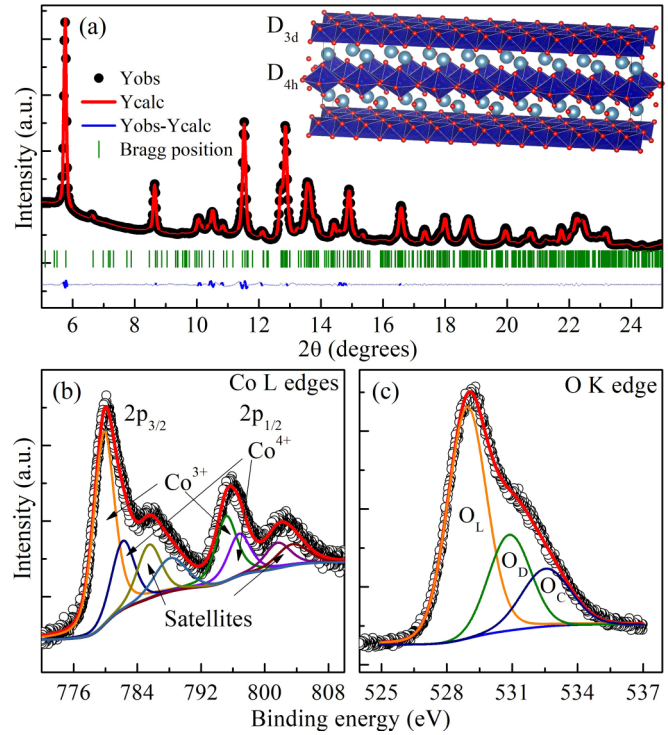

FIG. 1. (a) Rietveld refined XRD pattern with the supercell in inset showing cobalt sites in rocksalt and triangular layers. (b) Co $2p$ XPS spectra fitted with Co^{3+} and Co^{4+} components. (c) O $1s$ core XPS with lattice oxygen (O_L), deficient oxygen (O_D), and chemi-absorbed (O_C) oxygen features.

(GGA) calculations [13] concluded the Co^{3+} in HSS and Co^{4+} in intermediate spin state. To investigate spin states, we performed XAS measurements. This spectroscopy is able to probe spin states which appear in the multiplet feature(s) changes as the orbital occupation changes [18] as well as symmetry of crystal field [19]. Note that the orbital occupation depends upon the local symmetry around the metal ion. Usually, symmetry of octahedra depends on the type of connectivity. For example, corner-shared octahedra generally accept high symmetry (O_h or D_{4h}) while the edge-shared, low symmetry (D_{3d}). In the case of O_h symmetry, the resulting cubic crystal field splits the metal d orbitals into e_g and t_{2g} orbitals, which further splits into a_{1g}, b_{1g}, and e_g^{π}, b_{2g}, in a lower symmetry like D_{4h} (tetragonal crystal field). For the D_{3d} symmetry (trigonal crystal field) case, octahedra is compressed along the (111) direction [15] and degeneracy in e_g orbitals exists but t_{2g} splits into a_{1g} and e_g^{π}. It is known that the Co environment in the CoO_2 layer is in the D_{3d} symmetry and the rocksalt layers possess octahedra with distorted O_h symmetry [20]. Therefore, for the calculation of XAS patterns using the charge transfer multiplet simulation [21], we have considered the symmetry in the rocksalt as D_{4h}. Here we used the hopping parameters as $T_{eg} = 2$ eV and $T_{t2g} = 1$ eV and, to include the hybridization between states, we reduced the atomic multiplet to 80% (i.e., Slater integral F_{dd}=F_{pd}=G_{pd}=0.8). Distortion parameters D_s and D_t (for D_{4h}) and D_σ and D_τ (for D_{3d}) have been calculated from Δe_g and Δt_{2g} using relations reported elsewhere [19,22].

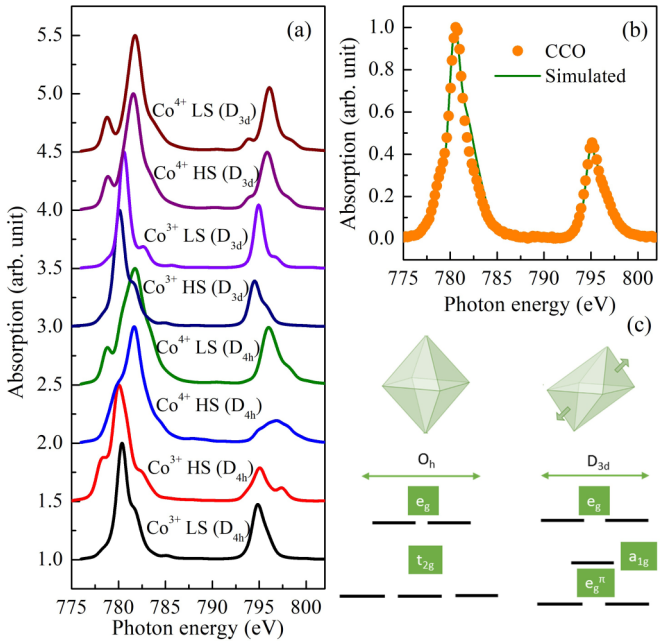

FIG. 2. (a) Simulated XAS spectra of Co^{3+} and Co^{4+} ions in HSS and LSS under D_{4h} and D_{3d} crystal fields. (b) Experimental and simulated XAS spectra of CCO. (c) Schematic of the crystal field effects in O_h and D_{3d} symmetries on degeneracy of d orbitals.

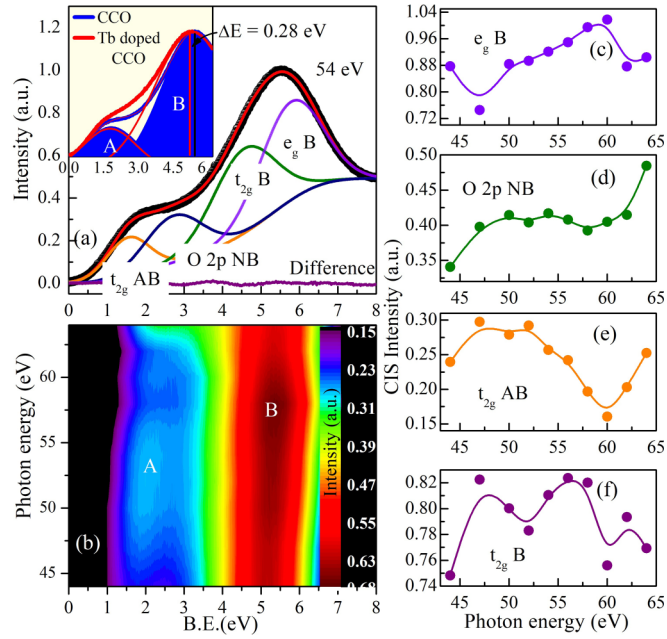

FIG. 3. (a) Fitted VBS with four bands of O_h symmetry (Ref. [12]), oscillations in the difference curve (fitted-measured) show the inconsistency of the model used. Inset shows the VBS of CCO and Tb-doped CCO, measured at 44 eV. (b) Contour plot of VBS measured at different energies (48–68 eV). (c)-(f) CIS plots for particular features in VBS.

Other parameters in the simulation are adopted from literature [23,24] and tabulated in Table S1 [6]. Figure 2(a) shows simulated XAS patterns for Co^{3+} and Co^{4+} in the LSS and HSS in D_{4h} as well as D_{3d} crystal-field symmetries. Figure 2(b) shows the experimentally observed XAS spectra and a simulated XAS spectra which is an iterative mixing of patterns shown in Fig. 2(a). A combination of Co^{3+}/Co^{4+} valencies and their spin states under D_{4h} and D_{3d} symmetries which resulted in the best fit [Fig. 2(b)] are tabulated in Table I. Note that this combination is obtained under the constraints that fractions of Co^{3+} and Co^{4+} are 68% and 32%, respectively, as observed from XPS.

Figure 3 shows the RPES results, the valence band spectroscopy in the $3p$-$3d$ resonance region (44-68 eV). In this energy interval, there may be two favorable excitations: first, direct photoemission and, second, super Coster-Kronig decay, which are given as $3p^63d^n + h\nu \longrightarrow 3p^63d^{n-1} + e^-$ and $3p^63d^n + h\nu \longrightarrow [3p^53d^{n+1}]^* \longrightarrow 3p^63d^{n-1} + e^-$, respectively, and the interference between these two give rise to resonance [25] in the intensity of $3d$ dominated bands in the valence band. Using the results of reported [12] $2p$-$3d$ RPES, we fitted the VBS using four peaks as t_{2g} antibonding (AB), $O\,2p$ nonbonding (NB), t_{2g} bonding (B), and e_g bonding (B). These assignments are made by assuming the O_h crystal field. Inadequate fitting [Fig. 3(a)] reveals the failure of this model. The constant initial state (CIS) plots show resonance and antiresonance features. Although these resonance and antiresonance are poorly visible, yet give hints of $3d$ dominance. Moreover, the contour plot [see Fig. 3(b)] clearly shows the two resonances at ~52.5 eV (feature A) and ~58 eV (feature B). These resonances are indispensable to symmetry-related information.

TABLE I. Concentration of Co ions with different spin states and valencies in D_{4h} and D_{3d} symmetry.

Ion	D_{4h}	D_{3d}
Co^{3+} HSS	20%	0
Co^{3+} LSS	14%	34%
Co^{4+} HSS	0	0
Co^{4+} LSS	32%	0

We propose that the valence band be defined by a combination of D_{4h} and D_{3d} crystal fields as observed from the XAS. But separation of these (D_{4h} and D_{3d}) in RPES is not feasible due to the resolution limitations. However, to include D_{3d} symmetry, the total number of participating orbitals must increase, as shown in Fig. 4(a). We have assigned six features as a_{1g} AB, e_g^π AB, $O\,2p$ NB, e_g^π B, a_{1g} B, and e_g B to define the VBS. In this model, the CIS plots [Fig. 4(c)] clearly show two resonances (corresponding to feature A and B) energies in $3d$ bands.

In the earlier reported model for the CoO_2 layer with O_h symmetry, the t_{2g}AB band is near E_F. However, in the present modified scheme of bands, the main contribution near E_F is from the a_{1g} AB band as shown in the CIS plot. Its resonance for photon energy ~52.5 eV confirms that feature A which corresponds to the triangular CoO_2 layer has dominant Co $3d$ character. Our observation is in agreement with the *ab initio* theory results [14] that the CoO_2 layer contributes DOS near the Fermi level. Resonance feature B, at a higher photon energy (~58 eV) is coming from the rocksalt layer. To confirm this, we have also recorded the VBS of Tb-doped

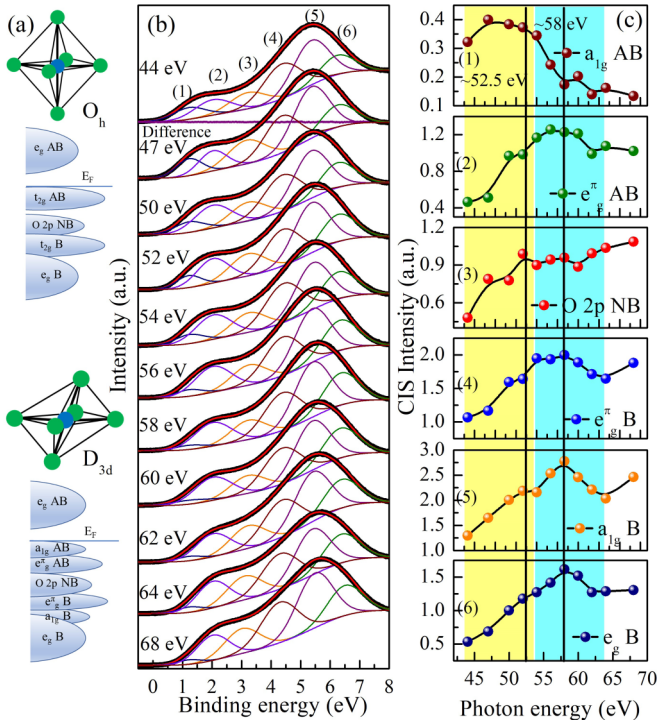

FIG. 4. (a) Schematic of regular octahedra in O_h symmetry and its effect on degeneracy on molecular orbitals and octahedra in D_{3d} symmetry and its associated molecular orbitals. (b) Fitted VBS spectra measured with different energies (across $3p$-$3d$ resonance), straight line behavior of difference curve (fitted-measured) shows the consistency of the model used and (c) CIS plots for particular features in VBS.

CCO ($Ca_{2.9}Tb_{0.1}Co_4O_9$). Tb doping at the Ca site will change the Co^{4+} into Co^{3+}. If it happens in the rocksalt layer, then this should result in feature B moving toward E_F by half of the crystal field difference between Co^{4+} (10Dq $\sim$ 2.4 eV) and Co^{3+} (10Dq $\sim$ 1.9 eV), which is $\sim$ 0.25 eV. Interestingly, we observe a shift of $\sim$ 0.28 eV in feature B of Tb-doped CCO while feature A remains unchanged [see inset of Fig. 3(a) to clearly visualize the shift in the positions; both spectra are fitted by a combination of two peaks]. This is direct evidence that feature B is coming from the rocksalt layer. This ultimately confirms the band-gap existence for the rocksalt subsystem as also reported by computational studies [14,15].

Note that earlier observation of the CoO_2 layer forming bands near E_F along with metal-like conduction in the *ab* plane of CCO [5] intuitively invited the proposals of S calculations based on the Boltzmann metallic conduction model [26]. However, this idea has not been found truly applicable by many authors [15,27] for the reason that the temperature dependence of high S in the high-temperature region is not as metal, rather flat (temperature independent). Moreover, the rocksalt layer offers a band gap and, for the band insulator, S $\propto (E_c - \mu)$ should contribute to the huge S with the decreasing trend with temperature ($S \propto \frac{1}{T}$), which is also not the case [28]. Aforementioned counterintuitive scenarios motivated researchers to use the Heikes formula for understanding the origin of the high Seebeck coefficient at higher temperatures.

In literature, many controversies exist regarding the band positioning of particular layers and S evaluation via the Heikes formula. Asahi *et al.* [13], using first-priniciples GGA, showed that CoO_2 states lie in the gap while the rocksalt contributes at the E_F. They calculated S in the rocksalt layer, which was 41 μV/K. Including correlation (DFT + U), Rébola *et al.* [14] found that CoO_2 is actually contributing at the E_F and rocksalt forms a gap, and they calculated S in the CoO_2 layer to be 227 μV/K. Soret and Lepetit [15], using cluster quantum chemical methods with correlation, supported the results of Rébola but estimated S as 125 μV/K in the CoO_2 layer using a nondegenerate character of a_{1g} orbitals. Our results related to electronic structures are consistent with these recent theoretical results but observation of the mixed valency in rocksalt layers motivates us to utilize the Heikes formula in rocksalt layers.

According to the Heikes formula, in the high-temperature limit, the thermopower can be written as [29] $S = \frac{-k_B}{e}\frac{\partial ln\, g}{\partial N}$; here k_B is the Boltzmann constant and e is the charge. Negative sign is because of the electron's negative charge. N represents the number of electrons and g represents the total number of configurations. Chaikin and Beni [29] have reported that spin degeneracy also plays an important role in determining the correct value of S. Aftwerward, Koshibae *et al.* [4] introduced the factor g_3/g_4, ratio of the degeneracy for different valencies (+3 and +4) to further improve the approximation to the S value. The modified formula is given by Eq. (1),

$$S = \frac{-k_B}{e} ln\left(\frac{g_3}{g_4}\frac{\eta}{1-\eta}\right), \tag{1}$$

where η represents the fraction of holes in the whole system. From the spectroscopic investigations, we have 14% Co^{3+} LSS, 20% Co^{3+} HSS, and 32% Co^{4+} LSS in the rocksalt layer (see Table I), which we denote as a, b, and c, respectively. Since these make total (100%) Co in rocksalt layer, the fractional concentration of Co^{4+} LSS can be represented as $x = c/(a+b+c) = 0.488$, Co^{3+} LSS as $y = a/(a+b+c) = 0.21$, and Co^{3+} HSS as $z = b/(a+b+c) = 0.3$. Utilizing Eq. (1) for two independent systems (Co^{3+} HSS-Co^{4+} LSS and Co^{3+} LSS-Co^{4+} LSS) and, assuming that the probability of hopping is equal for both Co^{3+} sites, one may use $\eta = x/2 = 0.242$. Using the two-site model [30] and the above configuration, one can calculate the Seebeck coefficient as $S = \frac{-k_B}{e}[(\frac{y}{y+z})ln(\frac{g_{3,\mathrm{LSS}}}{g_{4,\mathrm{LSS}}}\frac{\eta}{1-\eta}) + (\frac{z}{y+z})ln(\frac{g_{3,\mathrm{HSS}}}{g_{4,\mathrm{LSS}}}\frac{\eta}{1-\eta})]$, which results in S $\sim$115.2 $\mu V/K$. This value of S is in excellent agreement and closest to the experimental value [28,31] and validates our findings.

In conclusion, we have identified the symmetries around the Co ions in both subsystems, triangular and rocksalt, and quantified the spin states and valencies in each subsystem. RPES results manifest the existence of two Co sites in different environments by showing resonance from each subsystem. The calculated value of S, using the Heikes formula by including the obtained spin degeneracy, $\sim$ 115.2 μV/K, is in excellent agreement with the experiments. Our results confirm that the rocksalt layer is the main contributor to the high Seebeck coefficient value of this compound. Our experiments and results not only solve the pending and debated issue of origin

of the temperature-independent high Seebeck coefficient of this complex misfit $[Ca_2CoO_3]_{0.62}[CoO_2]$ cobaltate; also pave a way for spectroscopic solutions to complex compounds with nondegenerate sites and valencies.

The authors thankfully acknowledge R. J. Choudhary for providing the PES facility. Sharad Karwal and Rakesh Sah are acknowledged for their help during XPS/RPES and XAS measurements, respectively. The authors are grateful to Václav Petříček and Sander van Smaalen for stimulating discussions related to aperiodic structures. A.A., K.G., and D.K.S. acknowledge the DST-DESY project for financial support for performing experiments at PETRA III synchrotron. A.A. acknowledges UGC, New Delhi, India for providing financial support in the form of the MANF scheme (No. 2016-17/MANF-2015-17-UTT-53853). D.K.S. acknowledges financial support from DST-New Delhi, India through INT/RUS/RFBR/P-269.

[1] K. Takada, H. Sakurai, E. Takayama-Muromachi, F. Izumi, R. A. Dilanian, and T. Sasaki, Nature **422**, 53 (2003).
[2] J.-S. Kang, S. W. Han, T. Fujii, I. Terasaki, S. S. Lee, G. Kim, C. G. Olson, H. G. Lee, J.-Y. Kim, and B. I. Min, Phys. Rev. B **74**, 205116 (2006).
[3] R. E. Schaak, T. Klimczuk, M. L. Foo, and R. J. Cava, Nature **424**, 527 (2003).
[4] W. Koshibae, K. Tsutsui, and S. Maekawa, Phys. Rev. B **62**, 6869 (2000).
[5] A. C. Masset, C. Michel, A. Maignan, M. Hervieu, O. Toulemonde, F. Studer, B. Raveau, and J. Hejtmanek, Phys. Rev. B **62**, 166 (2000).
[6] See Supplemental Material at http://link.aps.org/supplemental/10.1103/PhysRevB.101.220202. Section I shows details about crystal structures. Section II shows magnetic and electrical characterization and Sec. III contains the table of parameters used for XAS simulations.
[7] Y. Miyazaki, M. Onoda, T. Oku, M. Kikuchi, Y. Ishii, Y. Ono, Y. Morii, and T. Kajitani, J. Phys. Soc. Jpn. **71**, 491 (2002).
[8] J. Sugiyama, H. Itahara, T. Tani, J. H. Brewer, and E. J. Ansaldo, Phys. Rev. B **66**, 134413 (2002).
[9] T. Mizokawa, L. H. Tjeng, H.-J. Lin, C. T. Chen, R. Kitawaki, I. Terasaki, S. Lambert, and C. Michel, Phys. Rev. B **71**, 193107 (2005).
[10] Y. Wakisaka, S. Hirata, T. Mizokawa, Y. Suzuki, Y. Miyazaki, and T. Kajitani, Phys. Rev. B **78**, 235107 (2008).
[11] G. Yang, Q. Ramasse and R. F. Klie, Phys. Rev. B **78**, 153109 (2008).
[12] T. Takeuchi, T. Kondo, T. Takami, H. Takahashi, H. Ikuta, U. Mizutani, K. Soda, R. Funahashi, M. Shikano, M. Mikami *et al.*, Phys. Rev. B **69**, 125410 (2004).
[13] R. Asahi, J. Sugiyama, and T. Tani, Phys. Rev. B **66**, 155103 (2002).
[14] A. Rébola, R. Klie, P. Zapol, and S. Öğüt, Phys. Rev. B **85**, 155132 (2012).
[15] J. Soret and M.-B. Lepetit, Phys. Rev. B **85**, 165145 (2012).
[16] M.-G. Kang, K.-H. Cho, J.-S. Kim, S. Nahm, S.-J. Yoon, and C.-Y. Kang, Acta Mater. **73**, 251 (2014).
[17] D. Grebille, S. Lambert, F. Bouree, and V. Petříček, J. Appl. Crystallogr. **37**, 823 (2004).
[18] A. Ahad, D. Shukla, F. Rahman, S. Majid, G. Okram, A. Sinha, D. Phase *et al.*, Acta Mater. **135**, 233 (2017).
[19] F. De Groot and A. Kotani, *Core Level Spectroscopy of Solids* (CRC Press, Boca Raton, Florida, 2008).
[20] N. Prasoetsopha, S. Pinitsoontorn, A. Bootchanont, P. Kidkhunthod, P. Srepusharawoot, T. Kamwanna, V. Amornkitbamrung, K. Kurosaki, and S. Yamanaka, J. Solid State Chem. **204**, 257 (2013).
[21] E. Stavitski and F. M. De Groot, Micron **41**, 687 (2010).
[22] M. W. Haverkort, arXiv:cond-mat/0505214.
[23] M. Merz, D. Fuchs, A. Assmann, S. Uebe, H. V. Lohneysen, P. Nagel, and S. Schuppler, Phys. Rev. B **84**, 014436 (2011).
[24] H.-J. Lin, Y. Y. Chin, Z. Hu, G. J. Shu, F. C. Chou, H. Ohta, K. Yoshimura, S. Hébert, A. Maignan, A. Tanaka, L. H. Tjeng, and C. T. Chen, Phys. Rev. B **81**, 115138 (2010).
[25] L. Davis, J. Appl. Phys. **59**, R25 (1986).
[26] J. M. Ziman, *Electrons and Phonons: The Theory of Transport Phenomena in Solids* (Oxford University Press, Oxford, London, 2001).
[27] R. F. Klie, Q. Qiao, T. Paulauskas, A. Gulec, A. Rebola, S. Öğüt, M. P. Prange, J. C. Idrobo, S. T. Pantelides, S. Kolesnik, B. Dabrowski, M. Ozdemir, C. Boyraz, D. Mazumdar, and A. Gupta, Phys. Rev. Lett. **108**, 196601 (2012).
[28] B. C. Zhao, Y. P. Sun, W. J. Lu, X. B. Zhu, and W. H. Song, Phys. Rev. B **74**, 144417 (2006).
[29] P. Chaikin and G. Beni, Phys. Rev. B **13**, 647 (1976).
[30] T. D. Sparks, A. Gurlo, M. W. Gaultois, and D. R. Clarke, Phys. Rev. B **98**, 024108 (2018).
[31] P. Limelette, V. Hardy, P. Auban-Senzier, D. Jérome, D. Flahaut, S. Hébert, R. Frésard, C. Simon, J. Noudem, and A. Maignan, Phys. Rev. B **71**, 233108 (2005).